



A new GPS/BDS tropospheric delay resolution approach for monitoring deformation in super high-rise buildings

Xin Li¹ · Guanwen Huang¹ · Qin Zhang¹ · Qingzhi Zhao²

Received: 2 April 2018 / Accepted: 19 June 2018 / Published online: 4 July 2018
© Springer-Verlag GmbH Germany, part of Springer Nature 2018

Abstract

A new approach for deformation monitoring of super high-rise building using GPS/BDS technology is proposed for the case when prior coordinates are known and the baseline is short but has a large height difference. The approach is based on the ambiguity function method (AFM). Considering that the double-differenced (DD) troposphere delay residual error cannot be ignored, the relative zenith tropospheric delay (RZTD) parameter is introduced into the original AFM equation. Thus, the RZTD and 3D coordinate parameters are together obtained through the modified AFM (MAFM). Due to the low computational efficiency of conventional AFM, an improved particle swarm optimization (IPSO) algorithm is used to search the four optimal parameters $X/Y/Z/RZTD$ and replaces the grid search method. In this study, GPS/BDS deformation monitoring data for buildings with approximately 290 m height difference were used to verify the feasibility of the proposed MAFM. Numerical results show a single-epoch average computation time of approximately 0.3 s, which meets the requirements of near-real-time dynamic monitoring. The average accuracy of the GPS single-epoch RZTD solution is better than 1 cm, the combined GPS/BDS MAFM performance outperforms the GPS-only system, and using multi-epoch observations can further improve the accuracy of the RZTD solution. After RZTD correction, GPS/BDS monitoring precision can be improved, particularly the height dimension, whose precision is improved by approximately 6 cm.

Keywords GPS/BDS · Super high-rise · Modified AFM (MAFM) · Relative zenith tropospheric delay (RZTD) · Improved particle swarm optimization (IPSO)

Introduction

Super high-rise buildings are an important aspect of modern cities and deformation monitoring is essential during both construction and completion (Huang et al. 2011; Xia et al. 2014). Due to its simple operation, all-weather availability, and high precision, GNSS technology is ideal for monitoring the deformation of super high-rise buildings. GPS/BDS super high-rise deformation monitoring generally adopts the relative positioning mode. Although the baseline between the reference and monitoring station is relatively short, the meteorological differences are often significant due to the large difference in height, and the

traditional double-difference (DD) mode cannot completely eliminate the effect of the tropospheric delay error (Dodson et al. 1996; Beutler et al. 1998). Thus, the influence of the residual troposphere delay must be taken into account when monitoring deformation in super high-rise buildings using GPS/BDS technology.

The tropospheric delay is generally divided into a hydrostatic delay and a wet delay. The former can be corrected by a precise model (Tralli and Lichten 1990), while the latter is mainly caused by atmospheric humidity, which is difficult to accurately model. In GPS/BDS data processing, we usually estimate the residual tropospheric delay using the least squares (LS) or extended Kalman filter (EKF) methods (Zhang and Lachapelle 2001; Yong et al. 2008). However, the relative zenith tropospheric delay (RZTD) is strongly correlated to height component, usually leading to the ill-conditioned problem in LS estimation, which seriously affects the result of the final height estimate (Li et al. 2010). In response to this problem, the negative impact can be somewhat reduced by long-term accumulated observations

✉ Guanwen Huang
huang830928@163.com

¹ College of Geology Engineering and Geomatics, Chang'an University, Xi'an 710054, Shanxi, China

² College of Geomatics, Xi'an University of Science and Technology, Xi'an 710054, Shanxi, China

(Dach et al. 2015). In fact, high-precision GPS research software such as GAMIT usually employs the residual troposphere delay parameter as a constant during a period of time (e.g., 2 h), and adopts the piece-wise linear (PWL) estimation strategy to reduce the influence of the residual troposphere error for long baseline resolution, usually with millimeter-level precision. Unfortunately, this does not meet the requirements of real-time single-epoch dynamic deformation monitoring.

Li et al. (2010) proposed a regularization method to achieve stable epoch solutions when conducting LS estimation. The method and experimental results were convincing, despite some complexity. Yong et al. (2008) estimated the RZTD and height parameter together and determined their correlation coefficient to separate RZTD and height; however, this method only specifies the correlation between RZTD and height, the correlations between the RZTD and the horizontal components are not adequately taken into account although they are relatively smaller. When conducting RZTD parameter estimation using EKF, a relatively accurate RZTD initial state value and variance should be provided. If the initial values are inaccurate, the convergence time might be long and the solution might not converge (Xu et al. 2013). In addition, to improve filtering precision and the ambiguity fixed rate, RZTD is generally assumed as the first-order Gauss–Markov random walk process (Takasu and Yasuda 2010). However, filtering RZTD solutions based on a random walk process cannot reflect real-time, real variations in the troposphere delay, especially when the troposphere delay changes suddenly due to atmospheric mutations or other outliers. Kim et al. (2004) used a forgetting factor to balance the RZTD estimate for the current epoch and the previously filtered resolution. This forgetting factor mainly depends on the temporal and spatial correlations; however, it should be empirically determined beforehand. Thus, this method cannot adapt to real-time true troposphere delay variations.

In many cases, GNSS deformation monitoring is essentially a quasi-static positioning process (Nickitopoulou et al. 2006); the monitoring station typically has relatively precise known coordinates, and relatively small amplitude variations over a short span. Therefore, the ambiguity function method (AFM) (Remondi 1984) based on the coordinate domain is a well-suited approach for GNSS deformation monitoring. The advantage of AFM is that it can achieve high positioning accuracy without intractable cycle slip detection and complex ambiguity resolution. However, the AFM performance is easily affected by the multipath and unmodeled errors (Mader 1990; Hedgecock et al. 2014). Fortunately, GPS/BDS survey receivers are usually used for deformation monitoring under a relatively good observation environment, so the multipath effect can be largely avoided. Generally, the deformation monitoring baseline is very short; thus, many error sources such as

the ionospheric delay and clock and orbital errors can be eliminated by the DD model. In addition, with the availability of multi-system and multi-frequency GNSS, an increased number of observations can further improve the AFM performance.

Unlike other deformation monitoring, the DD tropospheric residual error in super high-rise deformation monitoring cannot be neglected. Therefore, in this study, we first change the traditional AFM equation by adding a RZTD parameter, which will be searched together with the 3D coordinate parameters in a pre-determined four-dimensional search space, resulting in a modified AMF (MAFM). Considering the low computational efficiency of AFM with the conventional grid search method (Eling et al. 2013; Han and Rizos 1996), especially with an additional RZTD parameter, we adopt a new intelligent optimization search algorithm, namely particle swarm optimization (PSO) (Kennedy and Eberhart 1995; Clerc and Kennedy 2002), to replace the conventional grid search method. Because the searching results obtained by PSO algorithm are easy to fall into locally optimal resolution (Higashi and Iba 2003; Chen et al. 2016), we first improve the PSO algorithm by drawing on the idea of the genetic variation method (Shi et al. 2005). The particles are divided into three groups, i.e., optimal, suboptimal, and poor populations, and a random mutation is conducted with a certain probability for the optimal particles with the purpose of increasing the diversity of optimal particles. To further improve the search reliability of MAFM, a loose constraint on the baseline length is used to reduce the opportunity for multiple local optimal solutions. Compared with the conventional grid searching method, the improved PSO (IPSO) can significantly increase the computational efficiency of MAFM, and has a more elaborate search capability (Li et al. 2017).

The proposed MAFM for GPS/BDS super high-rise deformation monitoring is immune to cycle slips and, as a nonlinear parameter resolution method, it can avoid the ill-posed problems caused by the strong correlation between RZTD and the height component parameter in LS estimation. In addition, it only requires a relatively safe and reasonable pre-determined search space instead of a specific initial value; thus, to some extent, it can reduce the dependence on the initial state when conducting EKF estimation. The RZTD parameter can be resolved independently epoch by epoch; thus, on the condition of good observations, the MAFM is expected to adapt to sudden changes of tropospheric delay caused by typhoons, heavy rain, and other emergencies. In practice, if the weather status is relatively stable, the precision and reliability of the MAFM RZTD resolution can be further improved by multi-epoch accumulative observations when conducting GPS/BDS super high-rise deformation monitoring.

Methods

The GPS/BDS positioning model for monitoring deformation in super high-rise buildings is given first, especially the relative zenith tropospheric delay (RZTD) parameter estimation model. Then the modified AFM (MAFM) for RZTD resolution is investigated in detail. A new RZTD parameter is innovatively introduced into the conventional AFM equation; an improved PSO (IPSO) algorithm is proposed and applied to replace the conventional AFM grid search method, called MAFM. Finally we give the flowchart of the MAFM data process.

GPS/BDS DD observation equation for monitoring deformation in super high-rise buildings

GPS/BDS observations mainly include the pseudorange and carrier phase. In this study, only the high-precision carrier phase observation is used for GPS/BDS super high-rise deformation monitoring. The observation equation is as follows:

$$\phi_r^j = \rho_r^j + T_r^j - I_r^j + c\delta t_r^j + \lambda N_r^j + \epsilon_r^j \quad (1)$$

where ρ_r^j denotes the geometric range of the receiver–satellite $r - j$, T_r^j and I_r^j denote the tropospheric delay and ionospheric delay, δt_r^j denotes the receiver–satellite clock error, c denotes the speed of light, λ is the wavelength, denotes the carrier phase ambiguity, and $N_r^j \epsilon_r^j$ is the remaining error.

To simplify the data processing, the relative positioning model is typically used, canceling the residual ionospheric and clock errors. The tropospheric delay (T_r^j) cannot be eliminated thoroughly using the DD model because of the typically large height difference. Thus, the DD observation equation for deformation monitoring of super high-rise buildings is as follows:

$$\phi_{br}^{ij} = \rho_{br}^{ij} + \lambda N_{br}^{ij} + T_{br}^{ij} + \epsilon_{br}^{ij} \quad (2)$$

where the subscript b denotes the reference station, r denotes the monitoring station, the superscript i denotes the reference satellite, j denotes the non-reference satellite, $\rho_{br}^{ij} = \rho_r^j - \rho_b^i - (\rho_b^j - \rho_b^i)$ denotes the DD geometric range, N_{br}^{ij} denotes the DD ambiguity, and T_{br}^{ij} denotes the DD tropospheric delay. The empirical model, such Saastamoinen (1972), is usually first used to accurately correct the dry delay part; thus, the residual ionospheric delay is mostly the wet component and taken as a parameter to be estimated. Generally, the zenith tropospheric delay (ZTD) is introduced. The expression for T_{br}^{ij} is as follows:

$$T_{br}^{ij} = f_T(e_r^j)T_{z,r}^j - f_T(e_r^i)T_{z,r}^i - (f_T(e_b^j)T_{z,b}^j - f_T(e_b^i)T_{z,b}^i) \quad (3)$$

where T_z is the zenith tropospheric delay, f_T is the mapping function, and e is the elevation angle. Because the baseline

length is short, satisfying $e_b^i \cong e_r^i, e_b^j \cong e_r^j$, the average elevation angle, θ , is introduced to replace e . Thus, Eq. (3) can be expressed as:

$$T_{br}^{ij} = f_T(\theta^j)(T_{z,r}^j - T_{z,b}^j) - f_T(\theta^i)(T_{z,r}^i - T_{z,b}^i) \quad (4)$$

The relative zenith tropospheric delay (RZTD) is defined as $T_{z,br} = T_{z,r} - T_{z,b}$. The residual delay can be expressed as a function of RZTD and wet mapping function with the assumption of azimuthal symmetry:

$$T_{br}^{ij} = [f_T(\theta^j) - f_T(\theta^i)] \times T_{z,br} \quad (5)$$

where $f_T(\theta^j) - f_T(\theta^i)$ denotes the relative mapping coefficient.

Modified AFM (MAFM) with additional RZTD parameter

AFM is an ambiguity resolution (AR) method based on the coordinate domain. The basic idea is that, with a pre-determined searching space and searching step, by calculating the corresponding ambiguity function value (AFV) point by point, realizing the process of optimal coordinate search, only rounding is required to obtain the DD integer ambiguity solution. Figure 1 shows an example 2-D contour map of GPS/BDS AFV for one epoch. Because more observations are used for AFM, the multi-peak characteristic of the combined GPS/BDS AFV is not as obvious as in the GPS-only system. As a result, more observations generally translate to more reliable AFM performance.

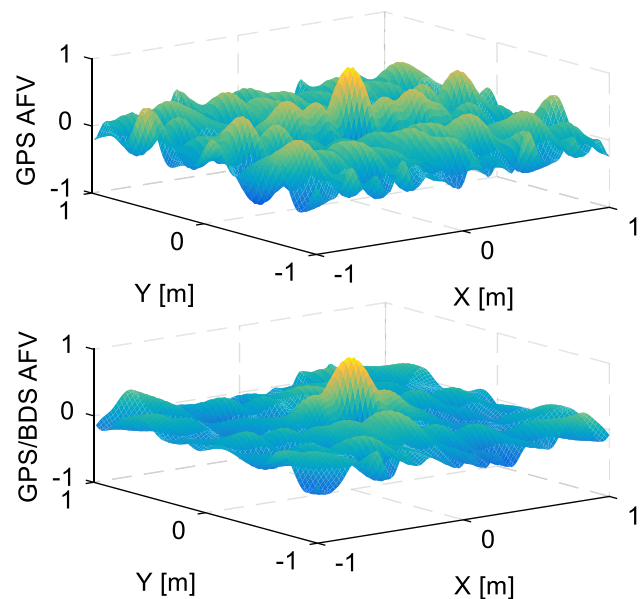


Fig. 1 2-D contour map of the GPS/BDS AFV for one epoch

As shown in (2), the DD observation equation still contains the DD tropospheric delay; therefore, we introduce the RZTD parameter into the original AFM equation, as follows:

$$AFV(X_r, Y_r, Z_r, T_{z,br}) = \frac{1}{n} \sum_{i=1}^n \cos 2\pi [\phi_{obs}^{br}(b|r) - \phi_{cal}^{br}(r|X_r, Y_r, Z_r, T_{z,br})] \quad (6)$$

where AFV denotes the ambiguity function value, X_r, Y_r, Z_r denote the 3D coordinate parameters, $T_{z,br}$ is the RZTD parameter, ϕ_{obs}^{br} denotes the DD observation, ϕ_{cal}^{br} is the calculated DD observation of the candidate points (corresponding to different X_r, Y_r, Z_r and RZTD values), and n denotes the total number of DD observations, including $n_i \geq 1$ epochs and n_f carrier frequencies ($1 \leq n_f \leq 3$). Within a pre-determined 4D searching space, if the searched candidate X_r, Y_r, Z_r and RZTD values are close to the truth value, then $\phi_{obs}^{br}[b|r] - \phi_{cal}^{br}[r|X_r, Y_r, Z_r, T_{z,br}]$ is also close to the correct ambiguity, considering the integer characteristics of the DD ambiguity. Thus, the AFV is close to 1 in such a case. In practice, due to the effect of observation noise and multipath, the AFV is usually less than 1.

PSO search method for improving MAFM efficiency

The point by point grid search method is usually of very low efficiency, which severely restricts AFM application. Since the modified AFM (MAFM) adds another parameter, the RZTD parameter, the conventional grid search method will be even more inefficient when applied to MAFM. Therefore, a new intelligent search algorithm, namely the particle swarm optimization (PSO) algorithm, is used to solve this problem effectively.

PSO algorithm overview

Particle swarm optimization (PSO) is derived from the study of bird predation. It employs information of individuals in shared groups so that the whole group’s motion can evolve from disorder to order in the problem-solving space, to obtain the optimal solution for the problem. For an N -dimensional space, the total population size is n . Assuming that $x_i = (x_{i1} \ x_{i2} \ \dots \ x_{iN})$, $u_i = (v_{i1} \ v_{i2} \ \dots \ v_{iN})$ denote the position vector and velocity vector of the particle i , respectively, the current optimal position of particle i denotes $pBest_i$, and the total population current optimal position denotes $gBest$. The standard PSO algorithm can be expressed as follows:

$$\begin{aligned} v_{in}^{(k+1)} &= \omega v_{in}^{(k)} + c_1 r_1 (pBest_{in}^{(k)} - x_{in}^{(k)}) + c_2 r_2 (gBest_n^{(k)} - x_{in}^{(k)}) \\ x_{in}^{(k+1)} &= x_{in}^{(k)} + v_{in}^{(k+1)} \end{aligned} \quad (7)$$

where the superscript k denotes the current iteration number and ω denotes the inertia weight. The particle self-cognitive part and the social-cognition part are balanced via the two learning factors, c_1 and c_2 . Random numbers between 0 and 1, r_1 and r_2 , are introduced to maintain the diversity of the group.

Looking at (7) and Fig. 2, the particle velocity update is mainly determined by three parts, i.e., the particle previous inertia velocity, the particle self-perception ($pBest_i$), and the social-perception part ($gBest$), by continuous iterative updating of particle $pBest_i$ and $gBest$ until a certain iterative convergence condition is satisfied.

The advantage of PSO is that it is easy to achieve and has a profound intelligence background. It is suitable for scientific research, particularly engineering applications. However, the PSO and other intelligent search algorithms are vulnerable to local optimization. To solve this problem, we first improve the PSO algorithm, and then employ the baseline length constraint to further enhance the reliability of PSO.

Improved PSO (IPSO) algorithm

Due to its fast convergence speed, and with a rapid decrease in population diversity, PSO easily represents the local optimum solution. Thus, the genetic variation method is introduced (Shi et al. 2005; Li et al. 2017). First, the particles are divided into three groups according to the fitness function value: optimal, suboptimal, and poor populations (S_1, S_2, S_3), then, a random mutation with a certain probability P_m is generated for S_1 . The random mutation can be expressed as

$$X_{id}^{k+1} = a_d + r_3(b_d - a_d) \quad (8)$$

where the subscript $d = (1, 2, \dots, N)$, a_d and b_d denote the parameter search upper and lower bounds, and r_3 is a random number between 0 and 1. With the random mutation, the population diversity is enhanced, and PSO reliability is improved to some extent, but the computation time is

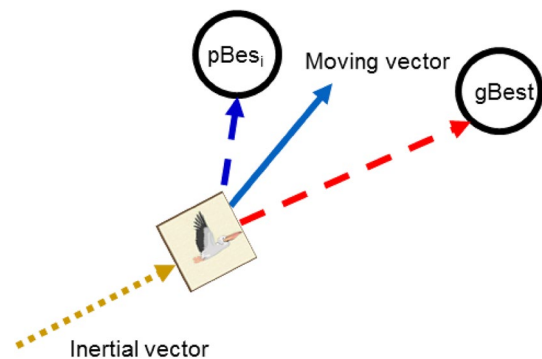


Fig. 2 Schematic diagram of particle evolution

increased. In practice, the P_m should be selected considering both search efficiency and reliability.

Baseline length constraint

Considering the deformation monitoring characteristics, generally, the monitoring station coordinates display relatively small variation amplitudes in a short time span, the baseline length constraint is used to improve the reliability of PSO search results further. The specific method is as follows:

$$AFV(X_r, Y_r, Z_r, T_{z,br}) = \frac{1}{n} \sum_{i=1}^n \cos 2\pi[\phi_{obs}^{br}(b|r) - \phi_{cal}^{br}(r|X_r, Y_r, Z_r, T_{z,br})] - \xi \tag{9}$$

where ξ denotes AFV attenuation, which can be obtained from the baseline length difference between the current epoch’s calculated baseline length computed with the searched $X_r/Y_r/Z_r/T_{z,br}$ solution and the previous epoch’s precise calculated baseline length. The specific expression is as follows:

$$\xi = \begin{cases} 0 & (\Delta l \leq \Delta l_t) \\ \alpha \cdot \Delta l & (\Delta l > \Delta l_t) \end{cases} \tag{10}$$

where Δl_t denotes the threshold of Δl and α denotes the attenuation factor.

For the PSO local optimal solution, after applying the baseline length constraint, the corresponding AFV is reduced to different extents; thus, the opportunity for local optimal solution is substantially reduced.

MAFM process

With GPS/BDS observations, the DD observation and relative mapping coefficient ($f_T(\theta^j) - f_T(\theta^i)$) are first obtained. Equation (9) shows the fitness function of IPSO. The MAFM convergence conditions are such that the difference in gBest corresponding parameters between two successive iterations is less than a given threshold ϵ . The specific MAFM process is as given in Fig. 3.

Experiments, results and analysis

The experiment was performed in Wuhan City, Hubei Province, on June 14, 2016, and fine weather conditions lasted during the entire observation session. The reference station S1 was installed on a low building approximately 16 m from the ground, reference station S2 was placed on the ground, and monitoring station S3 was installed on a super high-rise building approximately 290 m from the

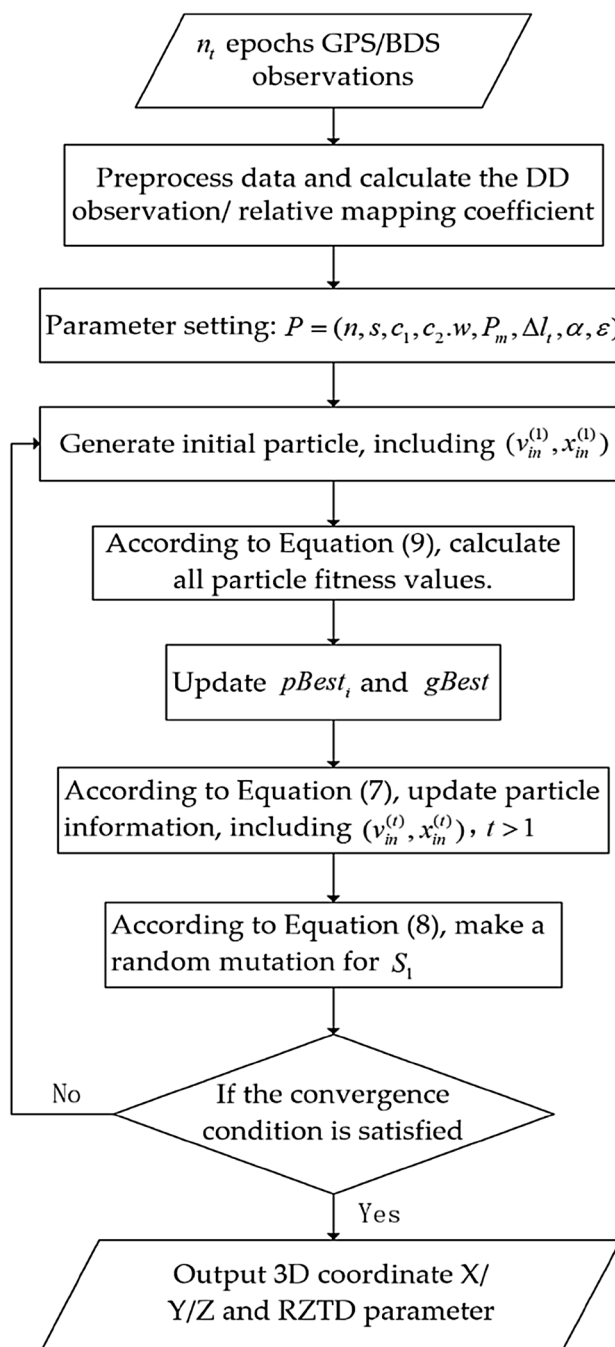


Fig. 3 Flowchart of MAFM

ground. The GPS/BDS multi-frequency observable signal was received by Trimble NETR9 boards. Figure 4 shows the experimental data acquisition scene and the baselines formed by S1/S2/S3 stations.

The observation lasted for approximately 7 h, the data sampling rate was 5 s, including approximately 5200 epochs, the cutoff elevation was set to 15°, and dual-frequency GPS/BDS data were used in the data processing.

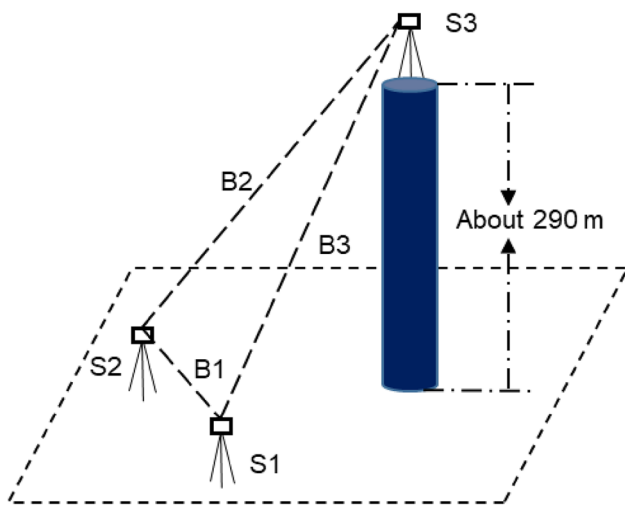


Fig. 4 Experimental data acquisition scene

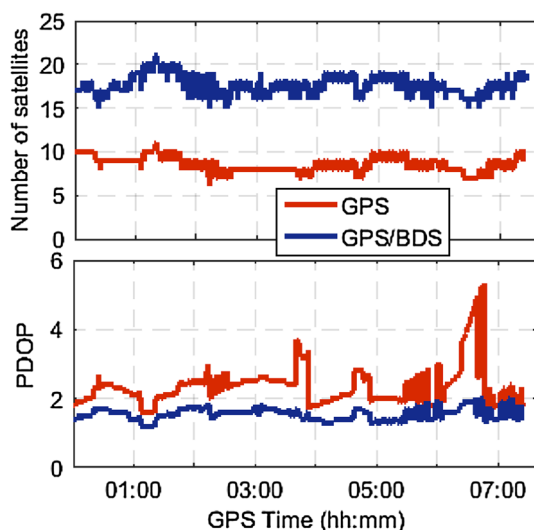


Fig. 5 Number of visible GPS/BDS satellites and PDOP values

Figure 5 shows the number of visible GPS/BDS satellites and PDOP value of monitoring station S3. These two indexes partly reflect the experimental environment. Compared with the GPS-only system, the combined GPS/BDS increases the number of visible satellites and improves the geometric satellite distribution.

Search procedure of IPSO

For the first epoch DD observation and the relative mapping coefficient of baseline B2, the IPSO is used to search for optimal S3 3D coordinates and B2 RZTD solutions. The initial prior coordinates of S3 are known, with an accuracy of better than 2 m. In this experiment, the search space is set to $[-2\text{ m}, 2\text{ m}]$, and the search space of the RZTD parameter is set to $[-0.1\text{ m}, 0.1\text{ m}]$. The IPSO parameters are set so that $P = (90, 30, 0.5, 0.5, 0.5, 0.6, 0.03, 3, 0.001)$. This ensures that the total number of particles is 90; the number of optimal (S_1), suboptimal (S_2), and poor (S_3) particles is 30; the two learning factors and the inertia weight are 0.5; the probability of the optimal particle (S_1) random mutation is 0.6; the baseline length constraint is 0.03 m; the AFV attenuation factor is 3; the particle convergence condition is that the corresponding parameter difference of gBest in two successive iterations is less than 0.001 m. In general, the larger the total number of particles, the higher the reliability of the search optimal solution, and lower the corresponding calculation efficiency. In practical applications, the efficiency and reliability should be considered before selecting the reasonable IPSO parameters.

According to the calculation flow introduced above, Fig. 6 shows the evolutionary (iterative) procedure of the four parameters, dX, dY, dZ, and RZTD. In the first iteration, the particles corresponding to the four parameters are generated randomly; thus, the global optimal particle (gBest) deviates from the true value. As the iterations increase, with continuous positioning and velocity updating of pBset and gBest, the positioning of gBest also trends gradually towards the truth value. Its corresponding AFV increases until the 28th iteration, satisfying the convergence condition. In other words, the difference in gBest (dX, dY, dZ, RZTD) between the last two iterations is less than 1 mm; therefore, in theory, the optimal search resolution of parameters using IPSO is higher than 1 mm. The entire search takes a total of 0.0981 s. In comparison, the conventional grid search method applied in Fig. 1, referring to a 2D search space $[-1\text{ m}, 1\text{ m}]$ only, with a search step of 0.005 m, the search time was 0.1739 s. Thus, the IPSO significantly improves MAFM efficiency and has a high search resolution.

MAFM result analysis

We use three baselines to verify the proposed MAFM, i.e., baseline B1, B2, B3 in Fig. 4. B1 is a short baseline on the ground, so in theory, the truth value of RZTD should be closer to 0, and the solved B1 RZTD is the accuracy of MAFM. The baseline height of B2 and B3 is close to each other. Thus, the truth value of the corresponding RZTD

Fig. 6 Evolution of the global optimal particle (gBest) 3D coordinate and RZTD

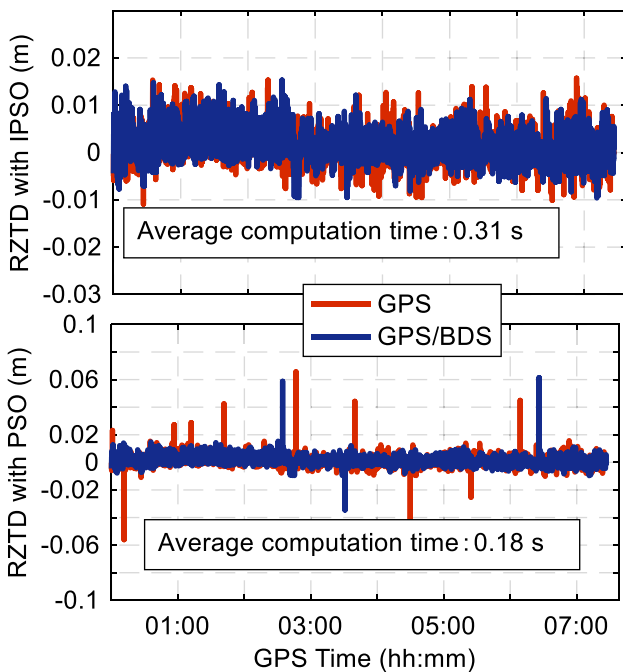
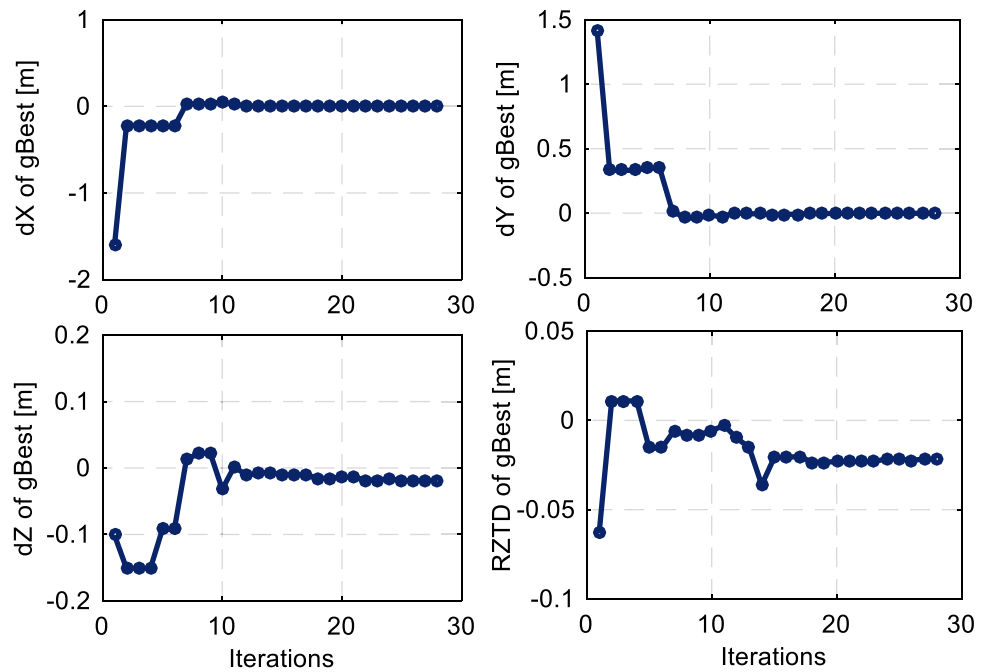


Fig. 7 B1 GPS/BDS single-epoch RZTD resolution using the IPSO (top) and PSO (bottom) searching method

should be almost the same, which can be an effective verification method for the MAFM RZTD resolution reliability. The influence of the resolved RZTD on monitoring precision is also analyzed.

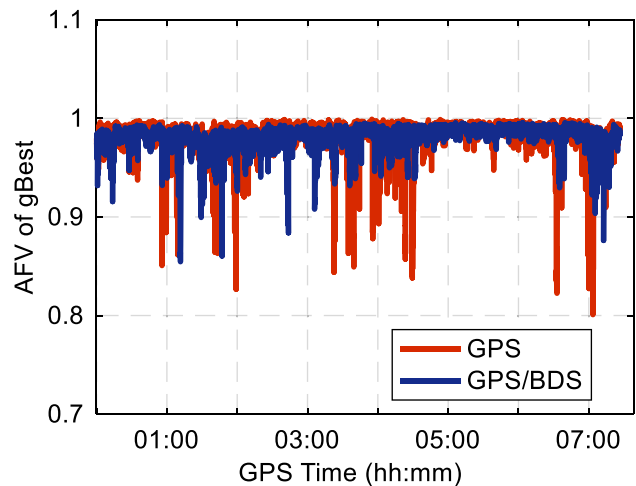


Fig. 8 GPS/BDS single-epoch gBest AFV

Baseline B1 validation

To verify the feasibility of MAFM, the baseline B1 is processed using MAFM. The total number of particles is set to 300, and the number of S_1, S_2, S_3 is 100, and other parameter settings are the same as above. Figure 7 shows the GPS/BDS MAFM single-epoch RZTD resolution using the IPSO and PSO searching method. The accuracy of the GPS MAFM RZTD solutions is better than 1 cm for most epochs, and the combined GPS/BDS solutions are further improved, with an average computation time of 0.31 s. Compared with the IPSO searching method, the PSO computational efficiency is higher; however, some jumps exist in the RZTD solutions,

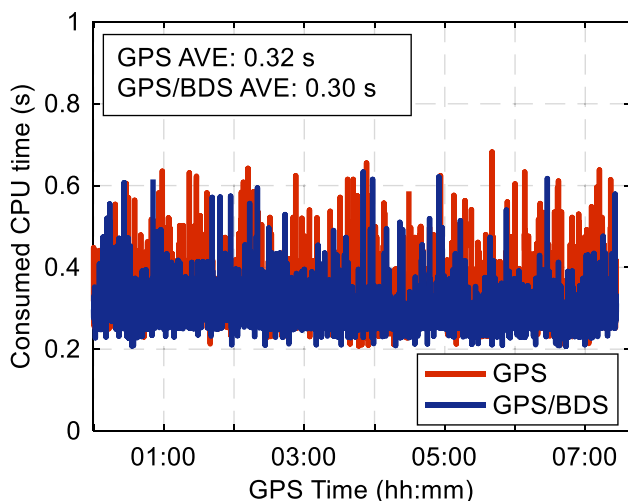


Fig. 9 GPS/BDS single-epoch computation time of MAFM

especially for the GPS-only system. This is due to the multi-peak characteristics of AFM, resulting in the PSO search falling into local optimum solutions on the RZTD jumping epochs. However, the IPSO conducts a random mutation with a certain probability for the optimal particle and increases the diversity of particles, and the additional baseline length constraint strategy can avoid the PSO falling into the locally optimal solution, although some computational efficiency is sacrificed.

Figure 8 shows the GPS/BDS corresponding AFV of gBest using MAFM epoch by epoch. The GPS AFV exceeds 0.97 for most epochs and, on these epochs, the combined GPS/BDS AFV is slightly lower than in the GPS-only system. This is because the BDS observation accuracy is currently slightly lower than that of GPS. As a result of an enlarged denominator n in (9), the corresponding AFV is also lower. For some epochs with heavy observation noise or multipath effects, the corresponding GPS AFV is reduced to a different extent. For these epochs, the combined GPS/BDS increases the number of observations and improves the geometric structure of the satellites, also improving MAFM reliability. Thus, the corresponding AFV increases to a different extent than the GPS-only system. Figures 7 and 8 indicate that epochs with low accuracy of the MAFM RZTD solution have a relatively low corresponding AFV. In fact, AFV can be used as a precision evaluation index for MAFM; generally, the higher the AFV, the higher the accuracy and reliability of the MAFM. Figure 5 shows that during the period from 5:00 to 6:00 the number of visible satellites is relatively large and the change of PDOP is relatively stable. Therefore, during this period, the corresponding AFV and accuracy of the MAFM RZTD solution are relatively high.

The computer processor used in our experiment is an “Intel(R) Pentium(R) CPU G620@2.60 GHz”, and the RAM

is 4.0 G. The entire program is written in standard C language. Figure 9 shows the single-epoch consumed CPU time of MAFM. The average GPS computation time is 0.32 s, although the combined GPS/BDS increases the DD observation, its corresponding average computation time is less than that of GPS. This is because the combined GPS/BDS multi-peak characteristic of MAFM is not as obvious as in the GPS-only system (Fig. 1), and it is easier to satisfy the iterative convergence condition; thus, the overall computation time is reduced. In fact, the efficiency of MAFM predominantly depends on the total number of particles and the convergence threshold. It is also partly related to the number of DD observations.

Under static conditions, the AFM reliability can be improved by accumulating observations. In our experiment, the monitoring of the super high-rise building is quasi-static positioning, so the 3D coordinates of the monitoring station and the relative tropospheric delay are expected to change slightly with time. The accuracy and reliability of the MAFM can, therefore, be improved using reasonable multi-epoch accumulative observations. Figure 10 shows the combined GPS/BDS MAFM results during 15 min of accumulative observation (a total of 180 epochs). The corresponding accuracy of the RZTD solution is further improved compared with the single-epoch solution. The average accuracy is 0.0013 m, and the maximum error is less than 0.005 m. Due to the increased number of DD observation during 180 epochs, the efficiency of MAFM is reduced, and the average computation time is 2.6864 s. In practical applications, the accumulative observation interval should be reasonably determined considering factors such as the prior regularity of deformation and the weather conditions.

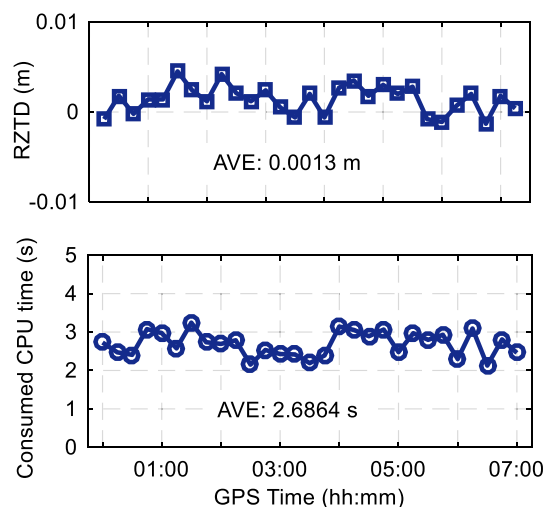


Fig. 10 B1 GPS/BDS MAFM results for 15 min of accumulative observations

Fig. 11 B2/B3 GPS/BDS single-epoch N/E/U solutions using MAFM

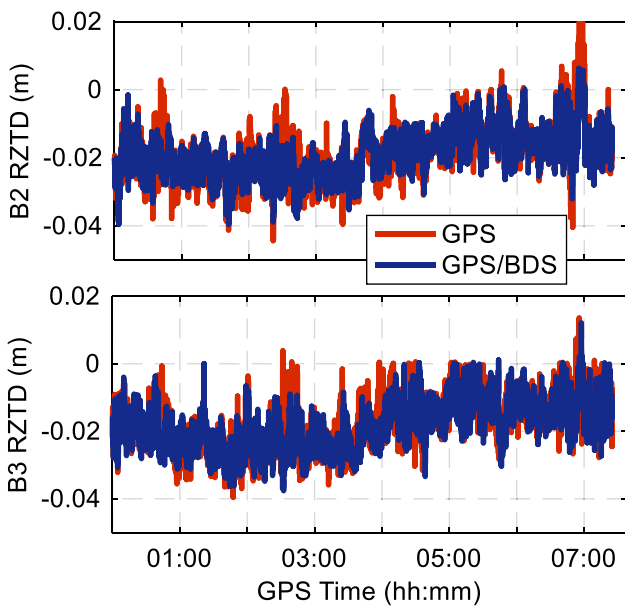
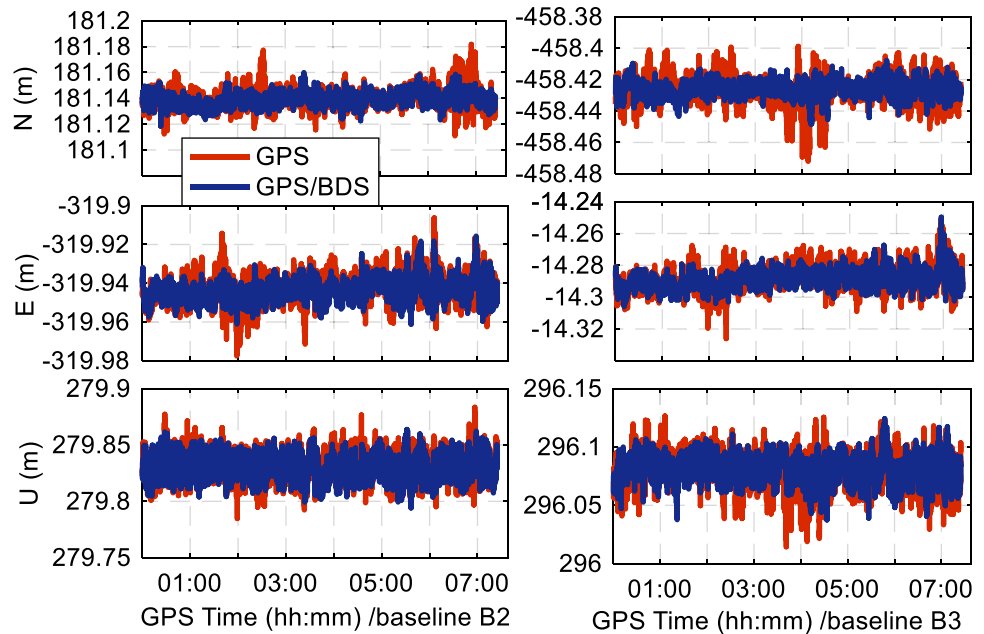


Fig. 12 B2/B3 GPS/BDS single-epoch MAFM RZTD solutions

Baseline B2/B3 validation

The baseline B2/B3 is processed to further verify the effectiveness of MAFM. All parameter settings are the same as above. Figure 11 shows the B2/B3 GPS/BDS single-epoch N/E/U baseline vector solution using MAFM. The fluctuation range of the plane N/E solutions is within 2 cm, and the height direction (*U*) is within 4 cm for most epochs. The combined GPS/BDS positioning accuracy outperforms that of the GPS-only system, especially under relatively poor

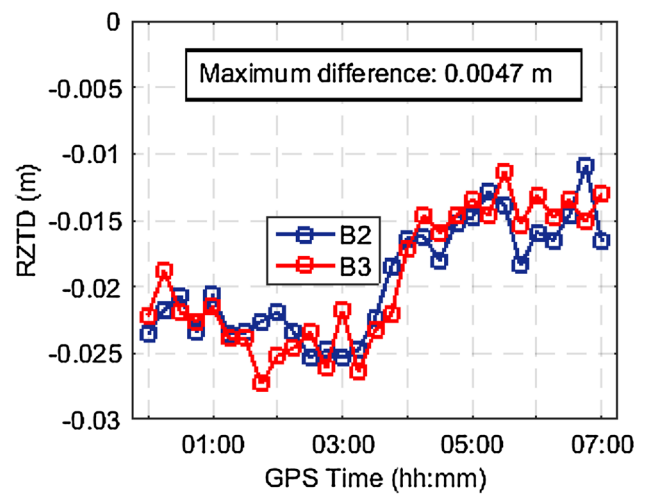


Fig. 13 B2/B3 GPS/BDS MAFM RZTD solutions with 15 min of accumulative observations

observation conditions. Considering the influence of GPS/BDS observation noise and the computed time sequence of the 3D N/E/U, the station S3 was determined to have no deformation during the entire monitoring period.

Figure 12 shows the B2/B3 GPS/BDS MAFM RZTD solutions epoch by epoch. As for the N/E/U solutions above, the combined GPS/BDS RZTD solutions outperform the GPS-only system. Both the value and variation trend of B2 GPS/BDS MAFM RZTD solutions agree well with those of B3, which indirectly proves the reliability of the MAFM RZTD solution. In sunny weather conditions, the RZTD can reach 2–3 cm. While for a rainy day, or for a baseline with a larger height difference, the RZTD is expected to be larger.

After mapping with the elevation angle, the DD troposphere residual delay is more significant. Therefore, the influence of the residual troposphere must be taken into account in high-precision GPS/BDS deformation monitoring of high-rise buildings.

Figure 13 shows the B2/B3-combined GPS/BDS RZTD solutions using MAFM with 15 min of accumulative observations. The RZTD solutions agree well with the single-epoch results shown in Fig. 12. The maximum difference between B2 and B3 solutions is only 0.0047 m. We propose that the precision of the inner coincidence of the MAFM RZTD solutions with 180 epochs of accumulative observations reaches millimeter levels in this experiment.

Influence of RZTD on monitoring precision

For GPS/BDS deformation monitoring of super high-rise buildings, the most interesting aspect is generally the monitoring precision of the 3D coordinates. In this study, the influence of the tropospheric residual error is taken into account in MAFM with the aim of improving the monitoring precision of super high-rise buildings. To analyze the influence of the residual tropospheric error on the 3D coordinate positioning result, we used KinPos software, developed by Wuhan University and based on LS estimation, to deal with the baseline B2 without considering the residual troposphere error. We then compared the final N/E/U values with the MAFM results, shown in Fig. 14. After residual tropospheric error correction, the MAFM corresponding 3D coordinate solutions are more stable. The difference between the MAFM and traditional LS solutions in the horizontal direction is slight; however, there is a systematic deviation in the height direction of up to approximately 6 cm. This systematic deviation is predominantly caused by the neglected tropospheric residual error.

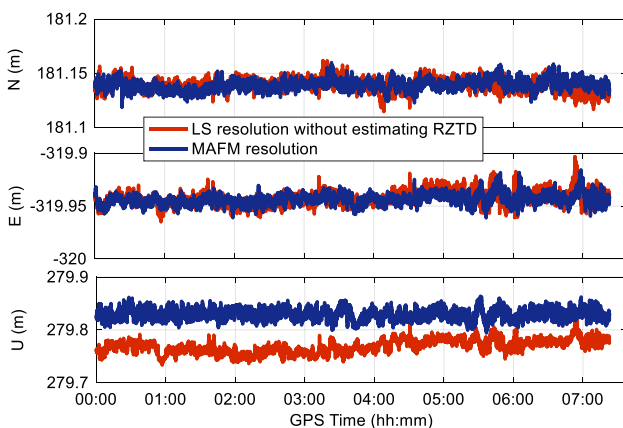


Fig. 14 Comparison of B2 GPS/BDS LS and MAFM N/E/U solutions

To quantitatively analyze the effect of the residual tropospheric error on the height direction, we make a seven-order polynomial fitting to the time series of the single-epoch MAFM RZTD solutions with B2-combined GPS/BDS data, and the positioning difference between the MAFM and LS solution in the *U* direction (*dU*), which are shown in Fig. 15. The temporal variation of the filtered RZTD is consistent with the filtered *dU*, showing a strong linear relationship. After calculation, the *dU* is approximately 3.14 times the RZTD, which is very consistent with the results of Dach et al. (2015) and Hong (2013). This demonstrates that, if the conventional short baseline positioning model is used to monitor the deformation of super high-rise buildings, the positioning result in the *U* direction will be approximately three times the systematic deviation of the RZTD. For urban super high-rise buildings, the RZTD errors are often up to decimeter level. With the residual tropospheric error correction using our proposed MAFM, the monitoring precision in the *U* direction can achieve decimeter-level improvements.

The optimal *X/Y/Z/RZTD* solutions are searched in a relatively large and safe 4D searching space. Therefore, it can somewhat reduce the dependence of the traditional EKF on the accuracy of the initial value. Moreover, the MAFM is expected to adapt better to sudden changes in the tropospheric delay, caused by typhoons, heavy rains, and other meteorological outliers, indicating the MAFM is more capable of achieving relatively reliable RZTD solutions epoch by epoch. However, the solutions obtained from the conventional random walk model used in EKF may deviate from the actual values, generally are lower, especially in the beginning period of these cases, because the estimated results of

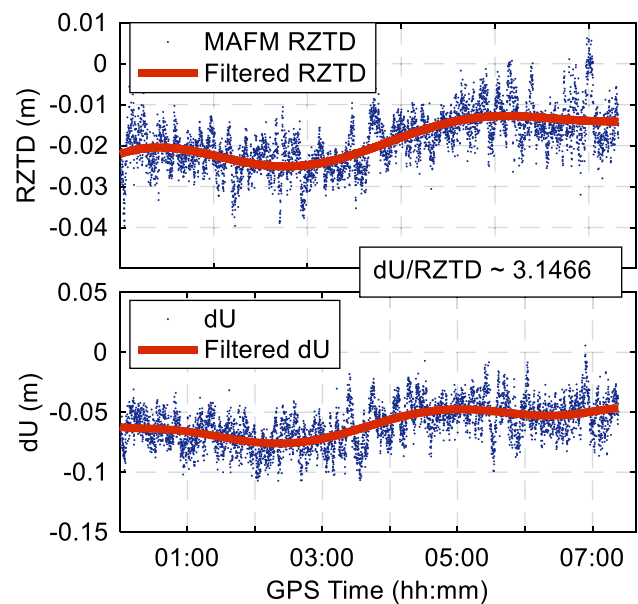


Fig. 15 Comparison of MAFM RZTD and *dU*

any two continuous epochs are not independent, with strong temporal correlation and spatial correlation. Unfortunately, there is a lack of monitoring data related to weather (RZTD) mutations. A possible advantage of MAFM in such cases was not reflected in our experiment.

Conclusions

We proposed a new GPS/BDS tropospheric delay resolution approach for monitoring deformation in super high-rise buildings, called MAFM. The optimal RZTD and 3D coordinate solutions are obtained within a pre-determined 4D searching space. An improved PSO searching method and a baseline length constraint are used to improve MAFM efficiency and reliability. The feasibility of MAFM is verified using measured GPS/BDS baselines with approximately 290 m height difference, and the following conclusions are obtained from the experimental results.

1. Compared with the conventional grid searching method, the efficiency of the $X/Y/Z/RZTD$ 4D search with IPSO is significantly improved. In addition, compared with the PSO algorithm, IPSO can improve the reliability of searching results, although it sacrifices some computational efficiency. The MAFM single-epoch average search time is approximately 0.3 s, which meets the requirements of near-real-time dynamic positioning for deformation monitoring.
2. The average accuracy of the MAFM GPS single-epoch RZTD solution is better than 1 cm. The combined GPS/BDS and reasonable multi-epoch accumulated observations can further improve MAFM accuracy and reliability.
3. Compared with the traditional short baseline positioning mode, after correcting for RZTD using MAFM, the monitoring precision for super high-rise buildings is improved, especially in the height direction, by approximately three times the RZTD.

Acknowledgements This work was supported by the Fundamental Research Funds for the Central Universities, Chang'an University, 2018 (No. 300102268102), the China Postdoctoral Science Foundation (No. 2018M633441), and the Programs of the National Natural Science Foundation of China (41790445, 41774025 and 41731066).

References

Beutler G, Bauersima I, Gurtner W, Rothacher M, Schildknecht T, Geiger A (1988) Atmospheric refraction and other important biases in GPS carrier phase observations. In: Atmospheric effects on geodetic space measurements. Monograph 12, School of Surveying, University of New South Wales, Sydney, pp 15–43

- Chen H, Li S, Liu J, Liu F, Suzuki M (2016) A novel modification of PSO algorithm for SML estimation of DOA. *Sensors* 16(12). <https://doi.org/10.3390/s16122188>
- Clerc M, Kennedy J (2002) The particle swarm-explosion, stability, and convergence in a multidimensional complex space. *IEEE Trans Evol Comput* 6(1):58–73
- Dach R, Lutz S, Walser P, Fridez P (2015) Bernese GNSS software version 5.2. User manual, Astronomical Institute, University of Bern, Bern Open Publishing
- Dodson AH, Shardlow PJ, Hubbard LCM, Elgered G, Jarlemark POJ (1996) Wet tropospheric effects on precise relative GPS height determination. *J Geod* 70(4):188–202. <https://doi.org/10.1007/BF00873700>
- Eling C, Zeimet P, Kuhlmann H (2013) Development of an instantaneous GNSS/MEMS attitude determination system. *GPS Solut* 17(1):129–138. <https://doi.org/10.1007/s10291-012-0266-8>
- Han S, Rizos C (1996) Improving the computational efficiency of the ambiguity function algorithm. *J Geod* 70(6):330–341
- Hedgecock W, Maroti M, Ledeczi A, Volgyesi P, Banalagay R (2014) Accurate real-time relative localization using single-frequency GPS. In: Proceedings of the 12th ACM conference on embedded network sensor systems, New York, November 03–06, 206–220
- Higashi N, Iba H (2003) Particle swarm optimization with Gaussian mutation. In: Proceedings of the IEEE 2013, Indianapolis, April 26–26, 72–79
- Hong CK (2013) Impact of tropospheric delays on the GPS positioning with double-difference observables. *J Korean Soc Surv Geod Photogramm Cartogr* 31(5):421–427. <https://doi.org/10.7848/ksgpc.2013.31.5.421>
- Huang Q, Xu B, Li B, Song GB, Teng J (2011) Monitoring for large cross-section CFSTs of a super high-rise building with piezoceramic actuators and sensors. *Adv Mater Res* 163–167:2553–2559. <https://doi.org/10.4028/www.scientific.net/AMR.163-167.2553>
- Kennedy J, Eberhart R (1995) Particle swarm optimization. In: Proceedings of the IEEE international conference on neural networks, Perth, November 27–December 1, pp 1942–1948
- Kim D, Bisnath S, Langley RB, Dare P (2004) Performance of long-baseline real-time kinematic applications by improving tropospheric delay modeling. In: Proceedings of ION GNSS 2004, Institute of Navigation, Long Beach Convention Center, September 21–24, pp 1414–1422
- Li B, Feng Y, Shen Y, Wang C (2010) Geometry-specified troposphere decorrelation for subcentimeter real-time kinematic solutions over long baselines. *J Geophys Earth*. <https://doi.org/10.1029/2010J B007549>
- Li X, Zhang P, Guo J, Wang J, Qiu W (2017) A new method for single-epoch ambiguity resolution with indoor pseudolite positioning. *Sensors* 17(4):921. <https://doi.org/10.3390/s17040921>
- Mader GL (1990) Ambiguity function techniques for GPS phase initialization and kinematic solutions. In: Proceedings of 2nd international symposium on precise positioning with the global positioning system, Ottawa, Canada
- Nickitopoulou A, Protopsalti K, Stiros S (2006) Monitoring dynamic and quasi-static deformations of large flexible engineering structures with GPS: accuracy, limitations and promises. *Eng Struct* 28(10):1471–1482. <https://doi.org/10.1016/j.engstruct.2006.02.001>
- Remondi B (1984) Using the global positioning system (GPS) phase observable for relative geodesy: modeling, processing, and results. University of Texas at Austin, Center for Space Research, Austin
- Saastamoinen J (1972) Atmospheric correction for troposphere and stratosphere in radio ranging of satellites. *Use Artif Satell Geod* 15:247–251

- Shi XH, Liang YC, Lee HP, Lu C, Wang L (2005) An improved GA and a novel PSO-GA-based hybrid algorithm. *Inf Process Lett* 93(5):255–261. <https://doi.org/10.1016/j.ipl.2004.11.003>
- Takasu T, Yasuda A (2010) Kalman-filter-based integer ambiguity resolution strategy for long-baseline RTK with Ionosphere and Troposphere Estimation. In: *Proceedings of ION GNSS 2010*, Institute of Navigation, Portland, September 21–24, pp 161–171
- Tralli DM, Lichten SM (1990) Stochastic estimation of tropospheric path delays in global positioning system geodetic measurements. *Bull Géod* 64(2):127–159
- Xia Y, Zhang P, Ni Y, Zhu H (2014) Deformation monitoring of a super-tall structure using real-time strain data. *Eng Struct* 67(10):29–38. <https://doi.org/10.1016/j.engstruct.2014.02.009>
- Xu Y, Cheng P, Cai Y (2013) Kalman filter algorithm for medium-range real-time kinematic positioning with one reference station. *J Southwest Jiaotong Univ* 48(2):317–322
- Yong WA, Kim D, Dare P, Park J (2008) Estimation of troposphere decorrelation using the combined zenith-dependent parameter. In: *Proceedings of ION GNSS 2008*, Institute of Navigation, Savannah, September 16–19, pp 261–270
- Zhang J, Lachapelle G (2001) Precise estimation of residual tropospheric delays using a regional GPS network for real-time kinematic applications. *J Geod* 75(5–6):255–266. <https://doi.org/10.1007/s001900100171>



Xin Li is a lecturer at Chang'an University, Xian, P.R. China. He received his Bachelor degree from Southwest Jiaotong University in 2011, received his M.Sc. and Ph.D. degrees in Surveying Engineering from Wuhan University, Wuhan, P. R. China, in 2013 and 2017. His research activities mainly include GNSS and precise indoor positioning.



Guanwen Huang is an associate professor of Chang'an University, Xian, P.R. China. He received Bachelor, M.Sc., and Ph.D. degrees in Surveying Engineering from Chang'an University, in 2005, 2008, and 2012. His research activities include Precise Point Positioning theory, real-time satellite clock model, and their application.



Qin Zhang is a professor of Chang'an University, Xian, P.R. China. She received Bachelor, M.Sc. and Ph.D. degrees in Surveying Engineering from Wuhan University, Wuhan, P. R. China, in 1982, 1994, and 2002. Her current research activities have been mainly related to GNSS and InSAR theory and application.



Qingzhi Zhao is a lecturer at Xi'an University of Science and Technology. He received B.Sc., Master's, and Ph.D. degrees in geodesy and surveying engineering from Shandong Agricultural University, Taian, China, China University of Mining and Technology, Xuzhou, China and Wuhan University, Wuhan, China, in 2011, 2014 and 2017, respectively. His research interests include global navigation satellite system atmospheric/meteorological studies, and GPS/MET and high-precision GPS

data processing.